Inorg. Chem. **2005**, *44*, 5001–5010

Corroborative Models of the Cobalt(II) Inhibited Fe/Mn Superoxide Dismutases

Marciela Scarpellini, Amy J. Wu, Jeff W. Kampf, and Vincent L. Pecoraro*

Willard H. Dow Laboratories, Department of Chemistry, University of Michigan, 930 North University, Ann Arbor, Michigan 48108

Received February 22, 2005

Attempting to model superoxide dismutase (SOD) enzymes, we designed two new N_3O-donor ligands to provide the same set of donor atoms observed in the active site of these enzymes: K^{i}Pr$_2$TCMA (potassium 1,4-diisopropyl-1,4,7-triazacyclononane-*N*-acetate) and KBPZG (potassium *N*,*N*-bis(3,5-dimethylpyrazolylmethyl) glycinate). Five new Co^{II} complexes (**1**–**5**) were obtained and characterized by X-ray crystallography, mass spectrometry, electrochemistry, magnetochemistry, UV–vis, and electron paramagnetic resonance (EPR) spectroscopies. The crystal structures of **1** and **3**–**5** revealed five-coordinate complexes, whereas complex **2** is six-coordinate. The EPR data of complexes **3** and **4** agree with those of the Co^{II}-substituted SOD, which strongly support the proposition that the active site of the enzyme structurally resembles these models. The redox behavior of complexes **1**–**5** clearly demonstrates the stabilization of the Co^{II} state in the ligand field provided by these ligands. The irreversibility displayed by all of the complexes is probably related to an electron-transfer process followed by a rearrangement of the geometry around the metal center for complexes **1** and **3**–**5** that probably changes from a trigonal bipyramidal (high spin, d^7) to octahedral (low spin, d^6) as Co^{II} is oxidized to Co^{III}, which is also expected to be accompanied by a spin-state conversion. As the redox potentials to convert the Co^{II} to Co^{III} are high, it can be inferred that the redox potential of the Co^{II}-substituted SOD may be outside the range required to convert the superoxide radical ($O_2^{\bullet -}$) to hydrogen peroxide, and this is sufficient to explain the inactivity of the enzyme. Finally, the complexes reported here are the first corroborative structural models of the Co^{II}-substituted SOD.

1. Introduction

Superoxide dismutases (SODs) are a class of metalloenzymes able to catalyze the dismutation of superoxide radicals into hydrogen peroxide using transition metals as cofactors (eqs 1 and 2).[1,2]

$$M^{3+} + HO_2^{\bullet} \rightarrow M^{2+} + O_2 \quad (1)$$

$$M^{2+} + HO_2^{\bullet} + 2H^+ \rightarrow M^{3+} + H_2O_2 \quad (2)$$

Presently, three types of SODs have been isolated: (i) metal-specific mononuclear, (ii) binuclear, and (iii) mononuclear cambialistic SODs. Metal-specific mononuclear SODs have been characterized as containing Fe,[3] Mn,[4,3k,3l] and Ni[5] in their active sites, while binuclear enzymes are known to present a Cu/Zn core.[6] Cambialistic SODs have been characterized as Fe- or Mn-containing enzymes and

* Corresponding author: vlpec@umich.edu; tel +11-734-7611519; fax +11-734-6474865.

(1) McAdam, M. E.; Fox, R. A.; Lavelle, F.; Fielden, E. M. *Biochem. J.* **1977**, *165*, 71−79.

(2) Stallings, W. C.; Metzger, A. L.; Pattridge, K. A.; Fee, J. A.; Ludwig, M. L. *Free Radical Res. Commun.* **1991**, *12*−*13*, 259−268.

(3) (a) Cooper, J. B.; McIntyre, K.; Badasso, M. O.; Wood, S. P.; Zhang, Y.; Garbe, T. R.; Young, D. *J. Mol. Biol.* **1995**, *246*, 531−544. (b) Lah, M. S.; Dixon, M. M.; Pattridge, K. A.; Stallings, W. C.; Fee, J. A.; Ludwig, M. L. *Biochemistry* **1995**, *34*, 1648−1660. (c) Cooper, J. B.; Saward S.; Erskine, P. T.; Badasso, M. O.; Wood, S. P.; Zhang, Y.; Young, D. *FEBS Lett.* **1996**, *387*, 105−108. (d) Lim, J.-H.; Yu, Y. G.; Han, Y. S.; Cho, S.-J.; Ahn, B.-Y.; Kim, S.-H.; Cho, Y. *J. Mol. Biol.* **1997**, *270*, 259−274. (e) Vance, C. K.; Miller, A.-F. *Biochemistry* **1998**, *37*, 5518−5527. (f) Buting, K.; Cooper, J. B.; Badasso, M. O.; Tickle, I. J.; Newton, I. J.; Wood, S. P.; Zhang, Y.; Young, D. *Eur. J. Biochem.* **1998**, *251*, 795−803. (g) Ursby, T.; Adinolfi, B. S.; Al-Karadaghi, S.; Vendittis, E. D.; Bocchini, V. *J. Mol. Biol.* **1998**, *286*, 189−205. (h) Kerfeld, C. A.; Yoshida, S.; Tran, K. T.; Yeates, T. O.; Cascio, D.; Bottin, H.; Berthomieu, C.; Sugiura, M.; Boussac, A. *J. Biol. Inorg. Chem.* **2003**, *8*, 707−714. (i) Yamakura, F.; Sugio, S.; Hiraoka, B. Y.; Ohmori, D.; Yokota, T. *Biochemistry* **2003**, *42*, 10790−10799. (j) Gogliettino, M. A.; Tanfani, F.; Sciré, A.; Ursby, T.; Adinolfi, B. S.; Cacciamani, T.; Vendittis, E. D. *Biochemistry* **2004**, *43*, 42199-2208. (k) For recent reviews: Miller, A.-F. *Curr. Opin. Chem. Biol.* **2004**, *8*, 162−168 (and references therein). (l) Whittaker, J. W. *Met. Ions Biol. Syst.* **2000**, *37*, 587−611 (and references therein).

10.1021/ic050281h CCC: $30.25
Published on Web 06/10/2005

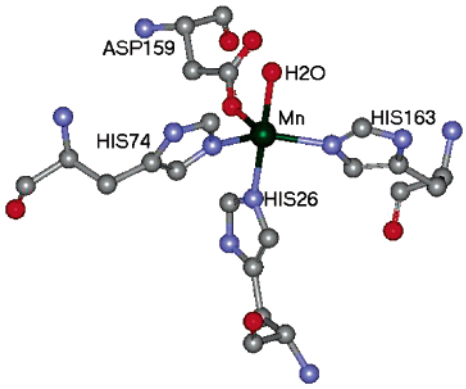

Figure 1. Cartoon of the active site structure of the human mitochondrial MnSOD based on coordinates from the PDB file (1N0J).[10]

are particularly interesting because of their ability to maintain their catalytic activity after the exchange between Mn and Fe ions. They have been isolated from some bacteria[7,8] and recently from seeds of a camphor tree.[9] Figure 1 shows the active site of the human mitochondrial Mn−SOD,[10] a Mn-specific enzyme in which the Mn^{III} ion is coordinated to three histidines (His163, His26, and His74), one aspartate (Asp159), and a hydroxo/water group (w400).[10]

X-ray crystallographic analyses of cambialistic SODs revealed high similarities to the metal-specific SODs. The structurally homologous active sites are composed of the metal center (Fe or Mn) surrounded by the same set of amino acids residues observed in Figure 1, in a distorted trigonal bipyramidal geometry.

As cambialistic SODs can be found containing either Fe or Mn, their interactions with several other metal ions have been reported.[7,8a,8b,11] Studies with the hyperthermostable Fe−SOD from the archaeon *Acidianus ambivalens* showed that the most effective metal replacement is achieved with Co^{II}, with an occupancy of 0.85 (±0.04) Co/monomer.[7] Kardinahl et al.[7] suggested that the preference for Co^{II} might be related to its ionic radius, which for five-coordinated ions is $Mn^{II} = 0.75$, $Fe^{II} \sim 0.70$, and $Co^{II} = 0.67$.[12] Although the active site has high affinity for Co^{II}, the Co-substituted enzyme (Co−SOD) is catalytically inactive. This inactivity has being explained based on the ligand field around the metal center and on its redox potential.[7] To be catalytically active, it has been proposed that the reduction potential of the Co−SOD has to be sufficiently positive in the Co^{III} state to accept one electron from the superoxide radical anion and negative enough to reduce the superoxide in the Co^{II} state.[3e,13] The reasons for the catalytic inactivity of Co−SOD are still unclear, as no redox potential data are available for Co−SOD and corroborative structural model complexes for this enzyme have not been reported.

We aimed to model structurally the active site of Fe/Mn SODs and have designed two new ligands (Chart 1) to provide the same set of donor atoms observed in the active site of these enzymes: three nitrogens and one oxygen from a carboxylate pendant arm. K^{i}Pr$_2$TCMA is a macrocyclic ligand based on 1,4,7-triazacyclononane, in which the cyclic nitrogen amines present two isopropyl substituent groups and one carboxylate moiety (Chart 1). KBPZG is a tripodal ligand containing as pendant arms two 3,5-dimethylpyrazole and a carboxylate group (Chart 1). Here, we present the syntheses and characterization of these new ligands and of five new cobalt complexes **1**−**5** (Chart 1), which are the first corroborative structural models for the active site of the Co-substituted Fe/Mn SODs. As azide has been shown to inhibit Fe/Mn SODs, complex **5** was synthesized to model structurally the azide-bound derivative of Fe/Mn SODs. Crystal structures of these inactivated azide SODs showed that upon azide coordination the active site becomes six-coordinate and confirmed that small molecules may bind to the active site, suggesting direct binding of superoxide to the metal site during the catalytic disproportionation cycle.[4a,3b]

2. Experimental Section

2.1. Abbreviations. TCMA, 1-acetato-1,4,7-triazacyclononane or 1,4,7-triazacyclononane-*N*-acetate; TACN, 1,4,7-triazacyclononane; K^{i}Pr$_2$TCMA, potassium 1,4-diisopropyl-1,4,7-triazacyclononane-

(4) (a) Schimidt, M.; Scherk, C.; Iakovleva, O.; Nolting, H. F.; Meier, B.; Parak, F. *Inorg. Chim. Acta* **1998**, *275*−*276*, 65−72. (b) Hsieh, Y.; Guan, Y.; Tu, C.; Bratt, P. J.; Angerhofer, A.; Lepock, J. R.; Hickey, M. J.; Tainer, J. A.; Nick, H. S.; Silverman, D. N. *Biochemistry* **1998**, *37*, 4731−4739. (c) Hearn, A. S.; Tu, C.; Nick, H. A.; Silverman, D. N. *J. Biol. Chem.* **1999**, *274*, 24457−24460. (d) Schwarts, A. L.; Yikilmaz, E.; Vance, C. K.; Vathyam, S.; Koder, R. L.; Miller, A.-F. *J. Inorg. Biochem.* **2000**, *80*, 247−256. (e) Hearn, A. S.; Stroupe. M. E.; Cabelli, D. E.; Lepock, J. R.; Tainer, J. A.; Nick, H. S.; Silverman, D. N. *Biochemistry* **2001**, *40*, 12051−12058. (f) Atzenhofer, W.; Regelsberger, G.; Jacob, U.; Peschek, G. A.; Furtmüller, P. G.; Huber, R.; Obinger, C. *J. Mol. Biol.* **2002**, *321*, 479−489. (g) Yu, J.; Yu, X.; Liu, J. *FEBS Lett.* **2004**, *562*, 22−26. (h) Davis, C. A.; Hearn, A. S.; Fletcher, B.; Bickford, J.; Garcia, J. E.; Leveque, V.; Melendez, J. A.; Silverman, D. N.; Zucalli, J.; Agarwal, A.; Nick, H. S. *J. Biol. Chem.* **2004**, *279*, 12769−12776. (i) Greenleaf, W. B.; Perry, J. P. Hearn, A. S.; Cabelli, D. E.; Lepock, J. R.; Stroupe, M. E.; Tainer, J. A.; Nick, H. S.; Silverman, D. N. *Biochemistry* **2004**, *43*, 7038−7045.
(5) (a) Kim, E.-J.; Kim, H.-P.; Hah, Y. C.; Roe, J. H. *Eur. J. Biochem.* **1996**, *241*, 178−185. (b) Youn H. D.; Kim, E. J.; Roe, J. H.; Hah, Y. C.; Kang, S. O. *Biochem. J.* **1996**, *318*, 889−896. (c) Barondeau, D. P.; Kassmann, C. J.; Bruns, C. K.; Tainer, J. A.; Getzoff, E. D. *Biochemistry* **2004**, *43*, 8038−8047.
(6) Strange, R. W.; Antonyuk, S.; Hough, M. A.; Doucette, P.; Rodriguez, J.; Hart, P. J.; Hayward, L. J.; Valentine, J. S.; Hasnain, S. S. *J. Mol. Biol.* **2003**, *328*, 877−891.
(7) Kardinahl, S.; Anemüller, S.; Schäfer, G. *Biol. Chem.* **2000**, *381*, 1089−1101.
(8) (a) Meier, B.; Gabbianelli, R. *J. Inorg. Biochem.* **1998**, *70*, 57−61. (b) Meier, B.; Sehn, A. P.; Sette, M.; Paci, M.; Desideri, A.; Rotilio, G. *FEBS Lett.* **1994**, *348*, 283−286. (c) Matsumoto, T.; Terauchi, T.; Isobe, T.; Matsuoka, K.; Yamamura, F. *Biochemistry* **1991**, *30*, 3210−3216. (d) Amano, A.; Shizukuishi, S.; Tamagawa, H.; Iwakura, K.; Tsunasawa, S.; Tsunemitsu, A. *J. Bacteriol.* **1990**, *172*, 1457−1463. (e) Pernnington, C. D.; Gregory, E. M. *J. Bacteriol.* **1986**, *166*, 528−532. (f) Martin, M. E.; Byers, B. R.; Oslon, M. O. J.; Salin, M. L.; Arceneaux, E. L.; Tolbert, C. *J. Biol. Chem.* **1986**, *261*, 9360−9367. (g) Gregory, M. E.; Drapper, C. H. *Arch. Biochem. Biophys.* **1983**, *220*, 293−300. (h) Meier, B.; Barra, D.; Bossa, F.; Calabrese, L.; Rotilio, G. *J. Biol. Chem.* **1982**, *257*, 13977−1398. (i) Schmidt, M., Meier, B.; Parak, F. *J. Biol. Inorg. Chem.* **1996**, *1*, 532−541. (j) Schmidt, M. *Eur. J. Biochem.* **1999**, *262*, 117−126. (k) Sugio, S.; Hiraoka, B. Y.; Yamakura, F. *Eur. J. Biochem.* **2000**, *267*, 3487−3495. (l) Yamakura, F.; Sugio, S.; Hiraoka, B. Y.; Ohmori, D.; Yokota, T. *Biochemistry* **2003**, *42*, 10790−10799.
(9) Chen, H.-Y.; Hu, R.-G.; Wang, B.-Z.; Chen, W.-F.; Liu, W.-Y.; Schröder, W.; Frank, P.; Ulbrich, N. *Arch. Biochem. Biophys.* **2002**, *404*, 218−226.
(10) Borgstahl, G. E. O.; Parge H. E.; Hickey, M. J.; Beyer, W. F.; Hallewell, R. A.; Tainer, J. A. *Cell* **1992**, *71*, 107−118.
(11) Renault, J. P.; Verchère-Béaur, C.; Morgenter-Badarau, I.; Piccioli, M. *FEBS Lett.* **1997**, *401*, 15−19.
(12) Shannon, R. D. *Acta Crystallogr.* **1976**, *A32*, 751−767.
(13) Barrette, W. C.; Sawyer, D. T.; Fee, J. A.; Asada, K. *Biochemistry* **1983**, *22*, 624−627.

Chart 1

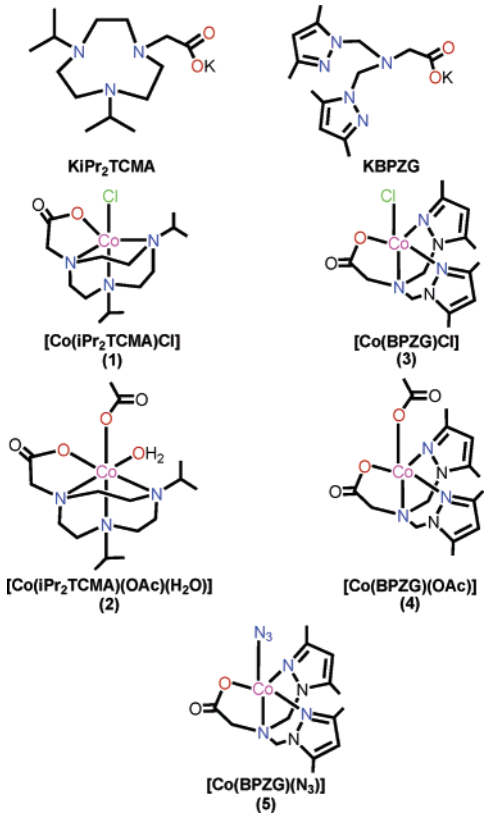

N-acetate; KBPZG, potassium *N*,*N*-bis(3,5-dimethylpyrazolylmethyl) glycinate; ^{i}PrOH, isopropyl alcohol; L4, racemic-4,5,7, 7,11,12,14,14-octamethyl-1,4,8,11-tetraazacbicyclo[6.6.2]-hexadecane; L1, 4,11-dimethyl-1,4,8,11-tetraazabicyclo[6.6.2]-hexadecane; L2, 4,10-dimethyl-1,4,7,10-tetraazabicyclo[6.5.2]-pentadecane; L3, 4,10-dimethyl-1,4,7,10-tetraazabicyclo[5.5.2]-pentadecane; L[5], *N*-(2-chloro-6-methylphenyl)pyridine-2-carboxamide; L[1], *N*-(2-picolinamido)phenyl)picolinamide; (*R*)-MeTACN, (−)-(*R*)-2-methyl-1,4,7-triazacyclononane.

2.2. Materials and Measurements. 1,4-Diisopropyl-1,4,7-triazacyclononane was synthesized as previously described.[14] All of the chemicals for syntheses and analyses were of analytical grade and were used without further purification. IR spectra (KBr pellet) were taken using a Perkin-Elmer Spectrum BX-FTIR spectrometer. Elemental analysis was performed using a Perkin-Elmer 2400 Series II Analyzer. Electrospray-ionization mass spectrometry (ESI-MS) spectra were recorded using a Micromass LCT time-of-flight mass spectrometer with electrospray and APCI, coupled to a Waters 1525 Binary HPLC pump. ^{1}H NMR and ^{13}C NMR were collected using a Varian Mercury 300 MHz NMR or a Varian Unity INOVA 400 MHz NMR spectrometer. UV−vis spectra were recorded using a Cary 100 Bio UV−visible spectrophometer. Cyclic voltammograms were recorded in acetonitrile using a BAS CV50W potentiostat at room temperature (22 ± 1 °C) and under argon atmosphere. A standard three-electrode cell was used, composed by the following electrodes: a glassy carbon working, a platinum auxiliary, and a Ag/AgCl reference. $TBAClO_4$ (0.1 mol·L^{-1}) was used as the supporting electrolyte and the ferrocenium−ferrocene couple[15] to monitor the reference electrode potential ($E_{1/2}$ = 390 mV vs Ag/AgCl). X-band electron paramagnetic resonance (EPR) spectra were recorded using a Bruker EMX electron spin resonance spectrometer with a Varian liquid N_2 cryostat or an Oxford Instruments liquid helium cryostat. Magnetic susceptibility data were obtained from the measured magnetic moment of powder samples collected using a Quantum Design MPMS Controller SQUID susceptometer (model 1822) equipped with a 5 T superconducting magnet. Measurements were taken over the temperature range of 5−300 K at a field of 2000 G. Diamagnetic corrections were performed using Pascal's constants.[16]

2.3. Syntheses. 2.3.1. Ligand Syntheses. (a) KiPr2TCMA Ligand. (i) 1-Ethyl Ester Acetate-1,4-diisopropyl-1,4,7-triazacyclononane. 1,4-Diisopropyl-1,4,7-triazacyclononane[14] (3.9 g, 18.3 mmol) and bromoacetic ethyl ester (2.0 mL, 18.3 mmol) were dissolved in 50 mL of methylene chloride and stirred for 15 min. Triethylamine (2.6 mL, 18.3 mL) was added dropwise, and the reaction mixture was stirred at room temperature for 45 h. The solution was stirred with decolorizing charcoal for 1 h, filtered, and combined with 50 mL of water. The organic layer was collected, and the aqueous solution was washed 3 times with 20 mL of methylene chloride. All of the organic layers were dried over sodium sulfate, filtered, and the solvent removed by rotatory evaporation to give an orange solid. The compound was obtained as a slightly yellow powder after washing with 200 mL of a methylene chloride/ethyl ether (1:20) solution and drying under reduced pressure. Yield: 4.6 g, 85%. ^{1}H NMR (300 MHz, $CDCl_3$): 4.15−4.19 (quartet, 2 H, $-O-CH_2$); 3.45 (s, 2 H, $-CH_2$); 2.70−3.40 (m, 14 H, $-CH_2$ + $-CH$); 1.19−1.21 (m, 15H, $-CH_3$) in ppm. Fourier transform Infrared spectroscopy (FTIR) (KBr, cm^{-1}): ν (C═O) 1737, ν (C−O) ∼1273, ν (C−N) 1076.

(ii) Potassium 1,4-Diisopropyl-1,4,7-triazacyclononane-*N*-acetate. A portion of 1-ethyl ester acetate-1,4-diisopropyl-1,4,7-triazacyclononane (3.0 g, 10 mmol) was added to a solution of potassium hydroxide (0.84 g, 15 mmol) in methanol (100 mL), and the reaction was stirred at room temperature overnight. The white powder was filtered off, washed with cold ethanol and diethyl ether, and dried under vacuum. Yield: 2.2 g, 70%. ^{1}H NMR (300 MHz, D_2O): 3.33 (s, 2 H, $-CH_2$); 3.28 (septet, 2 H, $-CH$); 2.94 (s, 4 H, $-CH_2$); 2.85 (s, 8 H, $-CH_2$); 1.19 (d, 12H, $-CH_3$) in ppm.^{13}C NMR (400 MHz, D_2O): δ 17.2 ($-CH_3$); 44.9, 46.4, 53.3 ($-CH_2-$N); 53.3 ($-CH$); 57.7 (N$-CH_2-$COO); 180.7 ($-$COO). FTIR (KBr, cm^{-1}): ν(C═O) 1657, ν(C−O) 1301, ν(C−N) 1091. ESI *m*/*z* (negative mode): 270.2 (100%), 271.2 (8%). Anal. Calcd for $KC_{14}N_3H_{28}O_2\cdot H_2O$ (Found): C, 51.34 (51.72); H, 9.23 (8.63); N, 12.65 (12.71).

(b) KBPZG Ligand. (i) *N*,*N*-Bis(3,5-dimethylpyrazolylmethyl)-glycyl Ethyl Ester. Triethylamine (2.2 mL, 17 mmol) was added to a suspension of glycine ethyl ester hydrochloride in anhydrous acetonitrile (2.1 g, 15 mmol, 40 mL) under stirring and N_2 atmosphere. The mixture was stirred for 5 min, and a solution of 3,5-dimethylpyrazol-1-methanol (3.8 g, 30 mmol, 50 mL of anhydrous acetonirile) was added dropwise under N_2. The reaction was allowed to stir for 3 days under N_2, and the solvent removed by reduced pressure evaporation. The product was dissolved in 10 mL of water, and the desired compound was extracted by washing 3 times with 30 mL of diethyl ether. The ether solution was washed with saturated brine solution and evaporated to dryness to yield the clear oil. Yield: 4.5 g, 93%. ^{1}H NMR (300 MHz, $CDCl_3$): 5.82 (s, 2 H, *H*−Pz); 5.05 (d, 4 H, $-CH_2$); 4.05−4.09 (quartet, 2 H,

(14) Mahapatra, S.; Halfen, J. A.; Wilkinson, E. C.; Pan, G.; Wang, X.; Young, V. G., Jr.; Cramer, C. J.; Que, L., Jr.; Tolman, W. B. *J. Am. Chem. Soc*. **1996**, *118*, 11555−11574.
(15) Gagné, R. R.; Koval, C. A.; Lisensky, G. C. *Inorg. Chem.* **1980**, *19*, 2854−2855.
(16) Kahn, O. *Molecular Magnetism*; VCH Publisher Inc.: New York, 1993; pp 3−4.

−O−CH_2); 3.47 (s, 2 H, −CH_2); 2.18 (d, 12 H, −CH_3) 1.25 (t, 3H, −CH_3) in ppm. ^{13}C NMR (400 MHz, $CDCl_3$): δ 10.9 (pz_{ring}−CH_3); 13.7 (O−CH_2−CH_3); 14.4 (pz_{ring}−CH_3); 50.7 (N−CH_2−COO); 60.9 (O−CH_2−CH_3); 65.2 (N−CH_2−pz_{ring}); 106.2 (−CH_{pzring}); 140.1 (−C_{pzring}−CH_3); 147.9 (−C_{pzring}−CH_3); 171.1 (−COO). FTIR (KBr, cm^{-1}): ν(C−H_{ar}) 2981−2900, ν(C═O) 1738, ν(C═N/C═C) 1557−1421, ν(C−O) 1297, ν(C−N) 1114, δ (C−H_{ar}) 733. Anal. Calcd for $C_{16}N_5H_{25}O_2$ (Found): C, 60.17 (59.32); H, 7.89 (8.10); N, 21.93 (21.89).

(ii) Potassium *N*,*N*-Bis(3,5-dimethylpyrazolylmethyl)glycinate. A solution of *N*,*N*-bis(3,5-dimethylpyrazolylmethyl)glycyl ethyl ester (4.8 g, 15 mmol, in 400 mL of anhydrous diethyl ether) was added dropwise to a solution of potassium trimethylsilanoate[17] (2.2 g, 15 mmol, in 100 mL of anhydrous diethyl ether) under N_2 and stirred vigorously. The reaction was stirred under N_2 for 3 h, and the white solid was filtered off and washed with anhydrous diethyl ether for several hours to afford the potassium salt of the ligand. Yield: 4.3 g, 87%. ^{1}H NMR (300 MHz, $CDCl_3$): 5.62 (s, 2 H, *H*−Pz); 4.79 (s, 4 H, −CH_2); 3.03 (s, 2 H, −CH_2); 2.00 (d, 12 H, −CH_3) in ppm. ^{13}C NMR (400 MHz, $CDCl_3$): δ 10.5 (pz_{ring}−CH_3); 13.3 (pz_{ring}−CH_3); 53.2 (N−CH_2−COO); 63.5 (N−CH_2−pz_{ring}); 105.2 (−CH_{pzring}); 140.4 (−C_{pzring}−CH_3); 147.6 (−C_{pzring}−CH_3); 176.3 (-COO). FTIR (KBr, cm^{-1}): ν(C−H_{ar}) 2981−2924, ν(C═O) 1580, ν(C═N/C═C) 1580−1466, ν(C−O) 1309, ν(C−N) 1119, δ (C−H_{ar}) 769. ESI *m*/*z* (negative mode): 290.2 (100%). Anal. Calcd for $C_{14}N_5H_{20}O_2K\cdot H_2O$ (Found): C, 48.40 (48.47); H, 6.38 (6.78); N, 20.16 (20.37).

2.3.2. Complexes Syntheses. [Co(^{i}Pr$_2$TCMA)Cl], Complex 1. Complex **1** was obtained by the reaction between methanolic solutions of the KiPr$_2$TCMA ligand (0.31 g, 1 mmol in 10 mL) and of $CoCl_2\cdot 6H_2O$ (0.26 g, 1 mmol in 10 mL). The reaction mixture was heated under stirring for ca. 30 min, until the volume of the solution was reduced to half. The white precipitate (KCl) was filtered, and isopropyl alcohol (5 mL) was added to the purple solution that was maintained at 22 °C for 1 week giving a purple precipitate. Purple single crystals suitable to X-ray crystallographic analysis were grown from an isopropyl alcohol solution. FTIR (KBr, cm^{-1}): ν(C−H) 2967−2875, ν_{asym}(C═O) 1650, ν_{sym}(C═O) 1497, ν(C−N) 1070, ν(C−O) 1318. ESI-MS *m*/*z* (positive mode) (CH_3CN): 329.2 (55%, [Co(^{i}Pr$_2$TCMA)]$^+$); 370.2 (100%, Co(^{i}Pr$_2$TCMA)(CH_3CN)]$^+$); 693.1 (15%, [Co$_2$(^{i}Pr$_2$TCMA)$_2$Cl]$^+$). Anal. Calcd for $CoC_{14}N_3H_{28}O_2Cl\cdot 1/2H_2O$ (Found): C, 44.99 (45.29); H, 7.82 (7.64); N, 11.24 (11.14).

[Co(^{i}Pr$_2$TCMA)(OAc)(H$_2$O)], Complex 2. Complex **2** was obtained by the same procedure described for complex **1**, employing $Co(OAc)_2\cdot 6H_2O$ instead of $CoCl_2\cdot 6H_2O$. Single crystals suitable for X-ray crystallographic analysis were obtained by recrystallization from a dilute ethyl acetate solution. FTIR (KBr, cm^{-1}): ν(C−H) 2960−2850, ν_{asym}(C═O) 1677/1603, ν_{sym}(C═O) 1497/1394, ν(C−N) 1103, ν(C−O) 1331. ESI-MS *m*/*z* (positive mode) (CH_3CN): 329.1 (64%, [Co(^{i}Pr$_2$TCMA)]$^+$); 370.2 (100%, [Co(^{i}Pr$_2$TCMA)(CH_3CN)]$^+$); 411.2 (12%, [Co(^{i}Pr$_2$TCMA)(CH_3CN)$_2$]$^+$); 717.3 (29%, [Co$_2$(^{i}Pr$_2$TCMA)$_2$(OAc)]$^+$). Anal. Calcd for $CoC_{16}N_3H_{33}O_5\cdot H_2O$ (Found): C, 45.28 (45.51); H, 8.31 (7.95); N, 9.90 (9.70).

[Co(BPZG)Cl], Complex 3. Complex **3** was obtained by the same procedure described above for complex **1**. Single crystals suitable for X-ray crystallographic analysis were obtained by recrystallization from an isopropyl alcohol solution. FTIR (KBr, cm^{-1}): ν(C−H_{ar}) 2960−2852, ν_{asym}(C═O) 1643, ν(C═N) 1550, ν(C═C) 1500−1430, ν(C−N) 1052, ν(C−O) 1286, δ (C−H_{ar}) 726. ESI-MS *m*/*z* (positive mode) (CH_3CN): 390.0 (100%, [Co(BPZG)(CH_3CN)]$^+$); 733.1 (42%, [Co$_2$(BPZG)$_2$(Cl)]$^+$). Anal. Calcd for $CoC_{14}N_5H_{20}O_2Cl\cdot 1/2H_2O$ (Found): C, 42.71 (42.43); H, 5.38 (5.35); N, 17.79 (17.63).

[Co(BPZG)(OAc)], Complex 4. Complex **4** was obtained by the same procedure described for complex **2**. Single crystals grown by recrystallization from a dilute ethyl acetate solution were suitable for X-ray crystallographic analysis. FTIR (KBr, cm^{-1}): ν(C−H_{ar}) 3000−2850, ν_{asym}(C═O) 1640/1611, ν(C═N) 1553, ν(C═C) 1496−1419, ν_{sym}(C═O) 1389, ν(C−O) 1257, ν(C−N) 1056, δ (C−H_{ar}) 730. ESI-MS *m*/*z* (positive mode) (CH_3CN): 390.0 (100%, [Co(BPZG)(CH_3CN)]$^+$); 757.2 (91%, [Co$_2$(BPZG)$_2$(OAc)]$^+$). Anal. Calcd for $CoC_{16}N_5H_{23}O_4\cdot 4H_2O$ (Found): C, 40.00 (40.74); H, 6.50 (6.02); N, 14.48 (14.43).

[Co(BPZG)N$_3$], Complex 5. Complex **5** was obtained by the reaction between methanolic solutions of the KBPZG ligand (0.33 g, 1 mmol in 10 mL) and $CoCl_2\cdot 6H_2O$ (0.26 g, 1 mmol in 10 mL). After 10 min, a solution of NaN_3 (0.065 g, 1 mmol in 10 mL of water) was added, and the reaction was heated under stirring for ca. 30 min, until the volume of the solution was reduced to half. After 3 days, a purple precipitate was isolated and recrystallized in ethyl alcohol affording crystals suitable for X-ray crystallographic analysis. FTIR (KBr, cm^{-1}): ν(C−H_{ar}) 2980−2924, ν(N_3) 2056, ν_{asym}(C═O) 1640, ν(C═N) 1549, ν(C═C) 1495−1524, ν(C−O) ~1290, ν(C−N) ~1054, δ (C−H_{ar}) 728. ESI-MS *m*/*z* (positive mode) (CH_3CN): 390.0% (100%, [Co(BPZG)(CH_3CN)]$^+$); 740.0 (11%, [Co$_2$(BPZG)$_2$(N_3)]$^+$). Anal. Calcd for $CoC_{14}N_8H_{20}O_2$ (Found): C, 42.97 (42.51); H, 5.15 (5.15); N, 28.64 (28.65).

2.4. Crystal Structure Determination. Crystals of complexes **1**−**5** were mounted on a standard Bruker SMART 1K CCD-based X-ray diffractometer equipped with a LT-2 low-temperature device and normal focus Mo-target X-ray tube (λ = 0.71073 Å) operated at 2000 W power (50 kV, 40 mA). The final cell constants (Table 1) were based on the *xyz* centroids of reflections above 10σ(*I*). Analysis of the data showed negligible decay during data collection; the data were processed with SADABS and corrected for absorption. The structures were solved and refined with the Bruker SHELXTL[18,19] (version 6.12) software package. All of the non-hydrogen atoms were refined anisotropically with the hydrogen atoms placed in idealized positions. The crystal of Complex **1** was determined to be a pseudomerhoedral twin with a derived twin law of (−1,0,0, 0,−1,0, 1,0,1) and twin fraction 0.369(2). Figures of the molecular structures were produce using the ORTEP program.[20] Further crystal structure and refinement data for all of the complexes are summarized in Table 1.

3. Results

3.1. Syntheses. KiPr$_2$TCMA was synthesized according standard procedures for obtaining macrocycle ligands. The cyclization reaction to obtain the intermediate 1,4,7-tris(*p*-toluenesulfonyl)-1,4,7-triazacyclononane followed the procedure previously described employing $CsCo_3$.[21] KBPZG was synthesized in two steps by the coupling reaction between

(17) Laganis, E. D.; Chenard, B. L. *Tetrahedron Lett.* **1984**, *25*, 5831−5834.

(18) Sheldrick, G. M. *SHELXTL*, version 6.12; Bruker Analytical X-ray: Madison, WI, 2001.

(19) Sheldrick, G. M. *SADABS*, version 2.10; Program for Empirical Absorption Correction of Area Detector Data, University of Gottingen: Gottingen, Germany, 2003; *Saint Plus*, version 7.01; Bruker Analytical X-ray: Madison, WI, 2003.

(20) Farrugia, L. J. *J. Appl. Crystallogr.* **1997**, *30*, 565.

(21) Iranzo, O.; Elmer, T.; Richard, J. P.; Morrow, J. R. *Inorg. Chem.* **2003**, *42*, 7737−7746.

Table 1. Crystallographic Data for Complexes **1**−**5**

	complex **1**	complex **2**	complex **3**	complex **4**	complex **5**
empirical formula	$C_{14}H_{28}ClCoN_3O_2$	$C_{16}H_{35}CoN_3O_6$	$C_{14}H_{20}ClCoN_5O_2$	$C_{16}H_{27}CoN_5O_6$	$C_{14}H_{20}CoN_8O_2$
formula weight	364.78	424.40	384.73	444.36	391.31
temperature (K)	113(2)	113(2)	123(2)	133(2)	123(2)
wavelength (Å)	0.71073	0.71073	0.71073	0.71073	0.71073
crystal system	monoclinic	monoclinic	monoclinic	triclinic	monoclinic
space group	$P2_1$	$C2/c$	$P2_1/c$	$P\bar{1}$	$P2_1/c$
unit cell dimensions					
a (Å)/α (deg)	6.8923(16)/90	30.357(3)/90	13.1603(15)/90	7.7740(8)/87.080(2)	13.0245(13)/90
b (Å)/β (deg)	12.138(3)/99.519(4)	8.1560(9)/107.095(2)	10.7582(12)/106.556(2)	10.7088(12)/86.868(2)	10.7195(10)/101.272(2)
c (Å)/γ (deg)	20.724(5)/90	16.9803(18)/90	12.1671(13)/90	12.7012(14)/74.185(2)	24.869(2)/
volume (Å^3)	1709.9(7)	4018.4(8)	1651.2(3)	1015.12(19)	3405.1(6)
Z/calcd density (mg/m^3)	4/1.417	8/1.403	4/1.548	2/1.454	8/1.527
abs coeff (mm^{-1})	1.167	0.890	1.217	0.887	1.035
F(000)	772	1816	796	466	1624
crystal size (mm)	0.44 × 0.06 × 0.06	0.44 × 0.38 × 0.07	0.40 × 0.14 × 0.06	0.42 × 0.40 × 0.20	0.60 × 0.10 × 0.07
θ range for data collection (deg)	2.99 to 28.43	2.97 to 28.36	3.23 to 28.29	2.90 to 28.31	3.14 to 28.30
limiting indices	$-9 \le h \le 9$ $-16 \le k \le 16$ $-27 \le l \le 27$	$-40 \le h \le 38$ $-10 \le k \le 10$ $-22 \le l \le 22$	$-17 \le h \le 16$ $-14 \le k \le 14$ $-16 \le l \le 16$	$-10 \le h \le 10$ $-14 \le k \le 14$ $-16 \le l \le 16$	$-17 \le h \le 17$ $-14 \le k \le 14$ $-33 \le l \le 33$
reflctns collected	8270	23409	16176	11904	34612
reflctns unique	4346 [R_{int} = 0.0507]	4988 [R_{int} = 0.0394]	4090 [R_{int} = 0.0349]	4972 [R_{int} = 0.0219]	8439 [R_{int} = 0.0392]
completeness to θ = 28.36	98.6%	99.4%	99.7%	98.4%	99.5%
abs correction			semiempirical from equiv		
max and min transmission	0.9333 and 0.6279	0.9403 and 0.6955	0.9306 and 0.6417	0.8425 and 0.7069	0.9311 and 0.5756
refinement method			full-matrix least-squares on F^2		
data/restraints/parameters	4346/0/196	4988/0/260	4090/0/212	4972/0/280	8439/0/459
goodness-of-fit on F^2	1.126	0.999	1.018	1.050	1.052
final R indices [$I > 2\sigma(I)$]	R_1 = 0.0617/ wR_2 = 0.1662	R_1 = 0.0321/ wR_2 = 0.0829	R_1 = 0.0301/ wR_2 = 0.0704	R_1 = 0.0297/ wR_2 = 0.0781	R_1 = 0.0397/ wR_2 = 0.0973
R indices (all data)	R_1 = 0.0756/ wR_2 = 0.1746	R_1 = 0.0464/ wR_2 = 0.0908	R_1 = 0.0440/ wR_2 = 0.0763	R_1 = 0.0337/ wR_2 = 0.0803	R_1 = 0.0588/ wR_2 = 0.1051
largest diff. peak and hole	1.186 and −1.109 e·Å^3	0.478 and −0.605 e·Å^3	0.349 and −0.265 e·Å^3	0.572 and −0.400 e·Å^3	1.074 and −0.556 e·Å^3

glycine ethyl ester and 3,5-dimethylpyrazol-1-methanol, followed by deprotection using potassium trimethylsilanoate.[17] Both ligands were obtained in good yields and in a purity grade for use without purification. These ligands were able to coordinate to Co^{II} in similar coordination modes yielding five- and six-coordinate complexes, as observed in the crystallographic analysis of all of the complexes. Elemental analyses show that complexes **1**, **3**, and **4** are hygroscopic.

IR spectroscopy was very useful as a preliminary characterization of ligands and complexes. In complexes **2** and **4**, the exogenous acetate coordination mode could be predicted by the difference between the asymmetric and symmetric stretches ($\Delta = \nu_{asym} - \nu_{sym}$). These bands were assigned by the difference spectra between the spectrum of **2** (or **4**) and **1** (or **3**). For both complexes, Δ values ∼200 cm^{-1} were determined, which are characteristics of monodentate acetate ligands.[22] For complex **5**, the presence of the azide group was unequivocally assigned by the sharp ν_{asym} stretching of the N_3 group at 2056 cm^{-1}, which is consistent with the presence of the terminally bonded azide.[22]

3.2. Crystal Structures of Complexes 1 and 2. Complex **1** forms purple crystals that belong to the monoclinic crystal system, space group $P2_1$. The crystallographic data and the main bond distances and angles for **1** are presented in Tables 1 and 2, respectively.

X-ray crystallographic analysis shows that the Co^{II} center in **1** (Figure 2) is five-coordinate in a distorted trigonal bipyramidal geometry ($\tau = 0.67$).[23] The three nitrogen atoms from the macrocyclic ligand $^{i}Pr_2$TCMA coordinate in such a way that the nitrogen atoms N2 and N3 lie in the trigonal plane at 2.134(4) and 2.154(4) Å, respectively. The third position in the plane is occupied by an oxygen atom (O1) from the carboxylate group, which is coordinated at 1.997(4) Å. The N1 nitrogen and the Cl1 chloride atoms are coordinated in the axial positions at 2.196(4) and 2.363(3) Å, respectively. Comparison between the C−O bond distances in the carboxylate group shows that they are nonsymmetric, where O2−C1 (1.220(6) Å) is shorter than O1−C1 (1.288(6) Å) and demonstrates the carboxyl (C═O) character of the O2−C1 bond.

Complex **2** crystallizes as pink crystals that belong to the monoclinic crystal system, space group $C2/c$. The crystallographic data and the main bond distances and angles for this complex are presented in Tables 1 and 2, respectively. Whereas in **1**, the Co^{II} center is five-coordinate, in **2** it is six-coordinate, with a distorted octahedral geometry (Figure 3). The three nitrogen atoms from the macrocyclic ligand $^{i}Pr_2$TCMA coordinate in a facial mode, where the atoms N1

(22) Nakamoto, K. In *Infrared and Raman Spectra of Inorganic and Coordination Compound*, 3rd ed.; part III; John Wiley & Sons: New York, 1977.

(23) Addison, A. W.; Rao, T. N.; Reedijik, J.; Vanrijin, J.; Verschoor, G. C. *J. Chem. Soc., Dalton Trans.* **1984**, 1349−1356.

Table 2. Bond Lengths (Å) and Angles (deg) for Complexes **1**−**5**

complex **1**		complex **2**		complex **3**		complex **4**		complex **5**[a]	
Co(1)−O(1)	1.997(4)	Co(1)−O(3)	2.0375(13)	Cl(1)−Co(1)	2.2908(5)	Co(1)−O(3)	1.9929(10)	Co(1)−O(1)	1.9809 (14)
Co(1)−N(2)	2.134(4)	Co(1)−O(1)	2.1227(12)	Co(1)−O(1)	1.9909(12)	Co(1)−O(1)	2.0053(11)	Co(1)−N(6)	1.9997 (19)
Co(1)−N(3)	2.154(4)	Co(1)−N(1)	2.1505(15)	Co(1)−N(4)	2.0501(15)	Co(1)−N(3)	2.0394(12)	Co(1)−N(3)	2.0358 (18)
Co(1)−N(1)	2.196(4)	Co(1)−O(5)	2.1697(13)	Co(1)−N(3)	2.0624(15)	Co(1)−N(5)	2.0561(13)	Co(1)−N(5)	2.0511(17)
Co(1)−Cl(1)	2.363(3)	Co(1)−N(2)	2.1940(15)	Co(1)−N(1)	2.2944(14)	Co(1)−N(1)	2.2870(12)	Co(1)−N(1)	2.2732 (16)
O(1)−C(1)	1.288(6)	Co(1)−N(3)	2.2391(15)	O(1)−C(1)	1.282(2)	O(1)−C(1)	1.2780(17)	O(1)−C(1)	1.281(2)
		C(1)−O(2)	1.257(2)	O(2)−C(1)	1.227(2)	O(2)−C(1)	1.2378(18)	O(2)−C(1)	1.231(2)
		C(1)−O(1)	1.265(2)						
		C(9)−O(4)	1.250(2)						
		C(9)−O(3)	1.266(2)						
O(1)−Co(1)−N(2)	125.18(15)	O(3)−Co(1)−O(1)	88.33(5)	O(1)−Co(1)−N(4)	120.96(5)	O(3)−Co(1)−O(1)	100.12(4)	O(1)−Co(1)−N(6)	96.07 (7)
O(1)−Co(1)−N(3)	137.32(15)	O(3)−Co(1)−N(1)	160.03(6)	O(1)−Co(1)−N(3)	116.02(5)	O(3)−Co(1)−N(3)	106.68(5)	O(1)−Co(1)−N(3)	111.37 (7)
N(2)−Co(1)−N(3)	88.32(15)	O(1)−Co(1)−N(1)	76.36(5)	N(4)−Co(1)−N(3)	108.22(6)	O(1)−Co(1)−N(3)	125.08(5)	N(6)−Co(1)−N(3)	109.63 (8)
O(1)−Co(1)−N(1)	79.95(16)	O(3)−Co(1)−O(5)	87.81(5)	O(1)−Co(1)−Cl(1)	94.98(4)	O(3)−Co(1)−N(5)	103.22(5)	O(1)−Co(1)−N(5)	123.91 (6)
N(2)−Co(1)−N(1)	82.02(15)	O(1)−Co(1)−O(5)	84.31(5)	N(4)−Co(1)−Cl(1)	106.76(4)	O(1)−Co(1)−N(5)	110.55(5)	N(6)−Co(1)−N(5)	101.03 (8)
N(3)−Co(1)−N(1)	79.73(15)	N(1)−Co(1)−O(5)	103.09(5)	N(3)−Co(1)−Cl(1)	107.94(4)	N(3)−Co(1)−N(5)	108.62(5)	N(3)−Co(1)−N(5)	112.10 (7)
O(1)−Co(1)−Cl(1)	99.33(13)	O(3)−Co(1)−N(2)	115.39(5)	O(1)−Co(1)−N(1)	76.87(5)	O(3)−Co(1)−N(1)	177.00(4)	O(1)−Co(1)−N(1)	78.77 (6)
N(2)−Co(1)−Cl(1)	96.29(13)	O(1)−Co(1)−N(2)	154.23(5)	N(4)−Co(1)−N(1)	76.36(5)	O(1)−Co(1)−N(1)	77.44(4)	N(6)−Co(1)−N(1)	172.27 (8)
N(3)−Co(1)−Cl(1)	102.47(13)	N(1)−Co(1)−N(2)	82.32(5)	N(3)−Co(1)−N(1)	77.90(5)	N(3)−Co(1)−N(1)	76.25(5)	N(3)−Co(1)−N(1)	77.71 (6)
N(1)−Co(1)−Cl(1)	177.22(12)	O(5)−Co(1)−N(2)	86.61(5)	Cl(1)−Co(1) −N(1)	171.60(4)	N(5)−Co(1)−N(1)	76.20(5)	N(5)−Co(1)−N(1)	78.71 (6)
O(2)−C(1)−O(1)	126.1(5)	O(3)−Co(1)−N(3)	91.21(5)	O(2)−C(1)−O(1)	124.94(16)	C(1)−O(1)−Co(1)	121.00(9)	O(2)−C(1)−O(1)	125. 09 (18)
O(2)−C(1)−C(2)	119.4(5)	O(1)−Co(1)−N(3)	107.22(5)			O(2)−C(1)−O(1)	125.22(14)	N(8)−N(7)−N(6)	176.9(2)
O(1)−C(1)−C(2)	114.5(4)	N(1)−Co(1)−N(3)	81.38(6)			O(4)−C(15)−O(3)	124.10(15)		
		O(5)−Co(1)−N(3)	168.40(5)						
		N(2)−Co(1)−N(3)	83.37(5)						

[a] Average values.

and N2 are in the basal plane at 2.151 (2) and 2.194(2) Å, respectively. These nitrogen atoms are mutually trans to the O3 and O1 atoms. O1 is the carboxylate oxygen atom from the ligand $^{i}Pr_2TCMA$ and is located 2.123(2) Å from the Co^{II} center, whereas O3 is the oxygen atom from the exogenous acetate group coordinated in a monodentate fashion at 2.038(1) Å. The axial positions are occupied by N3 (2.239(2) Å) and O5 (2.169(1) Å) atoms, where O5 is from a water molecule. As observed for **1**, both carboxylate groups present nonsymmetric C−O bond distances (Table 2), which is probably because of hydrogen bond interactions observed with coordinated and solvate water molecules (Table S1).

3.3. Crystal Structure of Complexes 3−5. Complexes **3**−**5** form purple crystals belonging, respectively, to the following crystal systems (space groups): monoclinic ($P2_1/c$), triclinic ($P\bar{1}$), and monoclinic ($P2_1/c$). The crystallographic data and the main bond distances and angles are presented in Tables 1 and 2, respectively.

Crystallographic analysis of the three complexes shows the Co^{II} five-coordinate in a very similar arrangement (Figures 4−6). As observed for **1**, complexes **3**−**5** also contain the Co^{II} center in a slightly distorted trigonal bipyramidal geometry, as evidenced by the structural Addison parameter (**3**, $\tau = 0.84$; **4**, $\tau = 0.87$; **5**, $\tau = 0.81$), which is 1.0 for a perfect trigonal bipyramid and 0.0 for a perfect square pyramid.[23] In complex **3**, the trigonal plane is composed of the carboxylate oxygen atom (O1) coordinated at 1.991(1) Å and the two pyrazole nitrogen atoms N3 and N4 at 2.062(2) and 2.050(2) Å, respectively. The axial positions are occupied by the nitrogen of the tertiary amine (Co1−

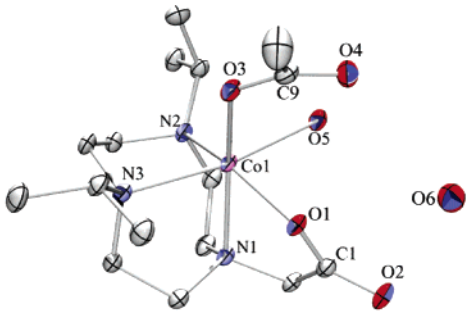

Figure 3. ORTEP[20] view of the complex **2**, showing the atoms labeling and the 50% probability ellipsoids.

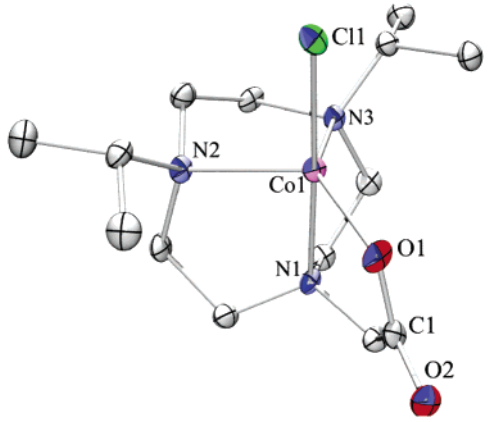

Figure 2. ORTEP[20] view of the complex **1**, showing the atoms labeling and the 50% probability ellipsoids.

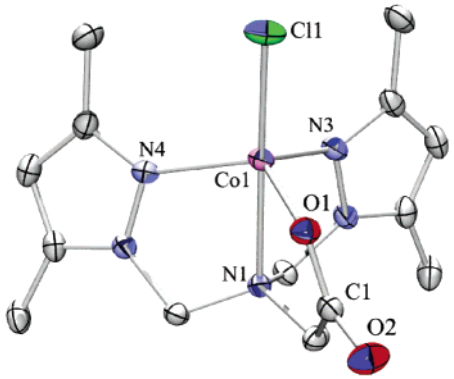

Figure 4. ORTEP[20] view of the complex **3**, showing the atoms labeling and the 50% probability ellipsoids.

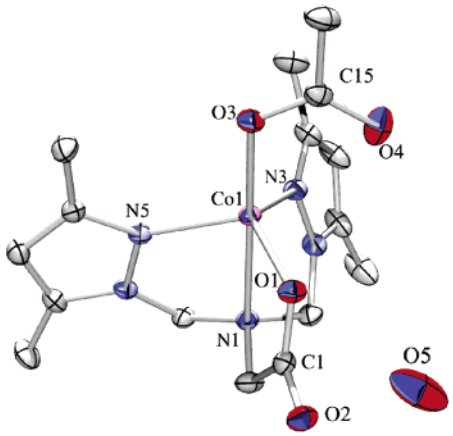

Figure 5. ORTEP[20] view of the complex **4**, showing the atoms labeling and the 50% probability ellipsoids.

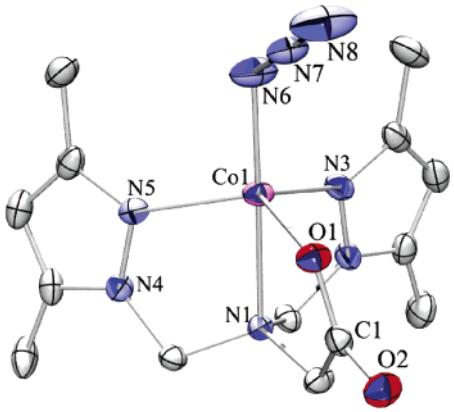

Figure 6. ORTEP[20] view of the complex **5**, showing the atoms labeling and the 50% probability ellipsoids.

N1 = 2.294(1) Å) and the chloride (Co1−Cl1 = 2.291(1) Å). As can be observed in Table 2, the Co−N_{amine}, Co−$N_{pyrazole}$, and Co−$O_{acetate}$ bond distances for **4** and **5** are similar to the values observed in **3**. Complex **4** differs from **3** by the presence of an acetate group coordinated in the axial position (Co1−O3 = 1.993(1) Å) instead of the chloride. As observed for **2**, complex **4** also exhibits hydrogen bond interactions between both acetate groups and a solvate water molecule (Table S1). Crystallographic analysis of **5** shows two independent, neutral molecules per unit cell, differing slightly from each other in angles and bond distances (Table 2). As cited before, the coordination sphere around the Co^{II} is very similar to **3** and **4**, differing by the presence of the azide group (Co1−N6 = 1.998(2) Å), which is coordinated in a linear form (N8−N7−N6 = 177.2(2) Å).

A comparison of these structural data shows that the Co−N_{amine} bond distances in the trigonal plane of **1** and **2** are longer than the Co−$N_{pyrazole}$ in complexes **3**−**5**. This fact should be expected as the pyrazole ring presents a greater π-bonding ability compared to alkylamines, which are exclusively σ-donors.

On the basis of the angles around the metal center (Table 2) and, consequently, the τ parameter (**1**, 0.81; **3**, 0.84; **4**, 0.87; **5**, 0.81), the $BPZG^-$ ligand is able to better accommodate the Co^{II} in a trigonal bipyramidal geometry than is the $^iPr_2TCMA^-$.

3.4. ESI-MS. Mass spectrometry in the ESI-positive mode spectra were recorded from freshly prepared solutions (methanol and acetonitrile) of complexes **1**−**5**, and the data are presented in the Experimental Section. All of the complexes present the base peak (100%) corresponding to the species containing one coordinated solvent molecule, $[Co(ligand)(solvent)]^+$. For complexes **1** and **2**, a peak at m/z^+ 329.2 is observed which is formulated as the species $[Co(^iPr_2TCMA)]^+$. The main feature in all of the spectra is a peak at $m/z^+ \sim 700$, which is assigned to the species $[Co_2(ligand)_2(X)]^+$, where X = Cl^-, OAc^-, or N_3^-. It is important to point out that peaks related to the fragmentation of the $^iPr_2TCMA^-$ or $BPZG^-$ ligands were not observed.

3.5. Magnetism and Spectroscopy. Magnetic and spectroscopic data are presented in Table 3. The magnetic susceptibilities for complexes **1**−**5** were collected from 300 to 5 K. Complexes **1** and **3**−**5** have μ_{eff} in the range of 3.66−4.50 μB at 300 K (Figure S1), which are in the range observed for other mononuclear Co^{II}, high-spin d^7 complexes.[12,24] The highest μ_{eff} value (4.56) was observed for complex **2**, which is typical of octahedral Co^{II} complexes with a high-spin d^7 configuration.[25]

The UV−vis spectra of complexes **1**−**5** were recorded in CH_2Cl_2, CH_3CN, and ^{i}PrOH/water (1:1) in the range of 300−900 nm, and the data are summarized in Table 3. Spectra obtained in CH_2Cl_2 (Figure 7) and CH_3CN are very similar. For all of the complexes, the visible spectra are characterized by bands with low molar absorptivity coefficients indicating ligand field (d−d) transitions. Complex **5** presents an additional band around 320 nm (ϵ = 1565 mol·L^{-1}·cm^{-1}), which can be assigned to the charge transfer related to the azide group. The spectra of **1** and **3**−**5** present bands in the visible region similar to those observed for others five-coordinate Co^{II} complexes.[24,26] On the other hand, the spectrum of **2** is more typical of six coordinate Co^{II} complexes.[27] All of the complexes are stable in both solvents for a long period of time (more than a month). In a mixture of ^{i}PrOH/water (1:1) (Figure S3), the behavior of all of the complexes is very different than those in CH_2Cl_2, suggesting changes in the coordination geometry of the Co^{II} center. In this medium, the spectra of complexes **1** and **2** are very similar, exhibiting bands around 440, 540, and 680 nm with analogous molar extinction coefficient values (Table 3), which suggests a very similar environment for both complexes. This same behavior is also observed for complexes **3** and **4**, which present bands around 470, 510, 550, and 750 nm. It is interesting to point out that in both cases, complexes containing chloride (**1** and **3**) present higher molar extinction coefficient values that those with the acetate group (**2** and **4**).

EPR spectra were recorded from frozen solutions of complexes **1**−**5** in CH_2Cl_2/toluene (1:1) at 4 and 11 K, and the data are summarized in Table 3 and shown in Figure 8.

(24) Ciampolini, M.; Nardi, N. *Inorg. Chem.* **1966**, *5*, 41−44.
(25) Lodeiro, C.; Capelo, J. L.; Bértolo, E.; Bastida, R. *Z. Anorg. Allg. Chem.* **2004**, *630*, 1110−1115.
(26) Lever, A. B. P. *Inorganic Spectroscopy*; Elsevier Science Publishers B.V.: Amsterdam, The Netherlands, 1984; pp 491−493, 487.
(27) Bertini, I.; Luchimat, C. *Adv. Inorg. Biochem.* **1984**, *6*, 71−111.

Table 3. UV−vis, Redox Potential, and EPR and Magnetic Data for Complexes **1**−**5**

complex	medium	λ_{max}, nm (ϵ, $M^{-1}\cdot cm^{-1}$)	E^e (mV vs NHE)	g factors at 4 K (11 K)	μ_{eff} (μB) at 300 K (5K)
1	CH_3CN	452[a] (114); 510 (sh); 576 (287); 760 (54)	$E_c = +890$, $E_a = +210$		
	CH_2Cl_2	453[a] (52); 554 (sh); 578 (167); 770 (18)		$g_\perp = 7.1$ (7.0), $g_{\|} = 2.0$ (2.0)	
	^{i}PrOH/H_2O	440[a] (25); 495 (sh); 542 (46); 680 (14)		$g_1 = 2.1$ (2.1), $g_2 = 4.1$ (4.1), $g_3 = 6.4$ (6.3)	
	solid				3.65 (3.90)
2	CH_3CN	442[b] (44); 500 (sh); 552 (52); 640 (sh)	$E_c = +800$, $E_a = -130$		
	CH_2Cl_2	446[b] (25); 500 (sh); 520 (sh); 551 (32)		$g_1 = 1.8$ (1.8), $g_2 = 2.9$ (3.0), $g_3 = 4.3$ (4.3)	
	^{i}PrOH/H_2O	442[b] (22); 492 (sh); 542 (32); 690 (10)		$g_1 = 2.2$ (2.1), $g_2 = 3.9$ (4.1), $g_3 = 6.0$ (6.1)	
	solid				4.56 (4.04)
3	CH_3CN	496[a] (158); 544 (197); 592 (230); 617 (sh)	$E_c = +1200$, $E_a = +230$		
	CH_2Cl_2	504[a] (133); 546 (sh); 593 (255); 615 (sh)		$g_\perp = 5.2$ (5.1), $g_{\|} = 2.0$ (2.0)	
	^{i}PrOH/H_2O	470[a] (sh); 510 (63); 550 (sh); 760 (16)		$g_\perp = 4.3$	
	solid				4.42 (4.31)
4	CH_3CN	471[a] (122); 505 (122); 588 (127); 615 (sh); 750 (62)	$E_c = +1300$, $E_a = -11$		
	CH_2Cl_2	470[d] (sh); 505 (87); 589 (98); 615 (sh)		$g_\perp = 5.3$ (5.1), $g_{\|} = 2.0$ (2.0)	
	^{i}PrOH/H_2O	465[a] (sh); 507 (48); 55 (sh); 745 (17)		$g_\perp = 4.0$ (4.2)	
	solid				4.50 (4.13)
5	CH_3CN	318[c] (1565); 492 (164); 533 (183); 596 (380); 625 (sh)	$E_c = +910$, $E_a = -44$		
	CH_2Cl_2	324[c] (1865); 497 (134); 534 (164); 602 (448)		$g_\perp = 4.7$ (4.9), $g_{\|} = 2.0$ (2.0)	
	^{i}PrOH/H_2O	308[a] (sh); 516 (87); 580 (98); 770 (20)			
	solid				3.66 (4.08)

[a] $C = 1.0 \times 10^{-3}$ mol·L^{-1}. [b] $C = 5.2 \times 10^{-3}$ mol·L^{-1}. [c] $C = 5.4 \times 10^{-4}$ mol·L^{-1}. [d] $C = 2.0 \times 10^{-3}$ mol·L^{-1}. [e] Scan rate: 100 mV/s.

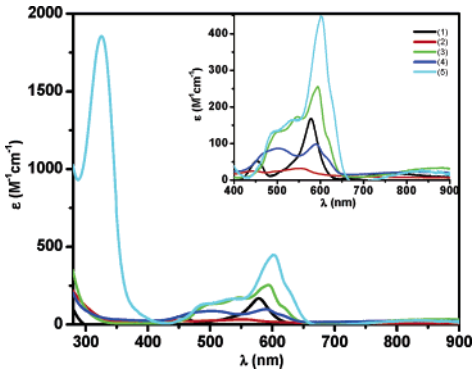

Figure 7. UV−vis spectra of complexes **1**−**5** in CH_2Cl_2 solutions: [complex] = 1×10^{-3} mol·L^{-1} for complexes **1** and **3**−**5** and 5×10^{-3} mol·L^{-1} for complex **2**.

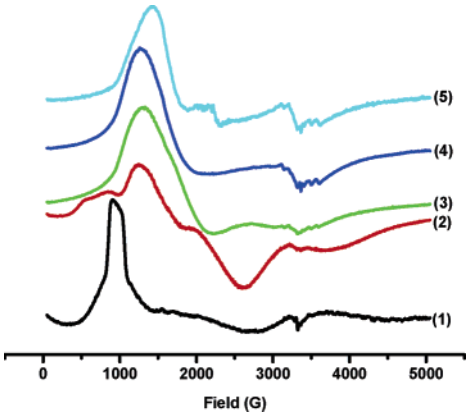

Figure 8. X-band EPR spectra of complexes **1**−**5** in CH_2Cl_2/toluene (1:1) solutions (1×10^{-3} mol·L^{-1}) at 4.5 K, recorded under the following conditions: microwave frequency, 9.424 GHz; microwave power, 2.02 mW; modulation frequency, 100.00 kHz; modulation amplitude, 10.00 G; receiver gain, 5.02×10^4; conversion time, 40.96 ms.

In CH_2Cl_2/toluene (1:1), the spectra of **1** and **3**−**5** are broad and axial with $g_{\|} \sim 2.0$ and $g_\perp \sim 5.0$, with complex **1** presenting a $g_\perp$ value around 7.0. The $g_{\|} \sim 2.0$ signals are split in an ill-resolved 8 line that may be characteristic of the hyperfine transition related to the ^{59}Co center (nuclear spin $^7/_2$). Complex **2** presents a broad rhombic spectrum of $g_1 \sim 1.8$, $g_2 \sim 2.9$, and $g_3 \sim 4.3$. All of the complexes were investigated at 4 and 11 K and decreases in the intensities of resonances with increasing temperature were observed.

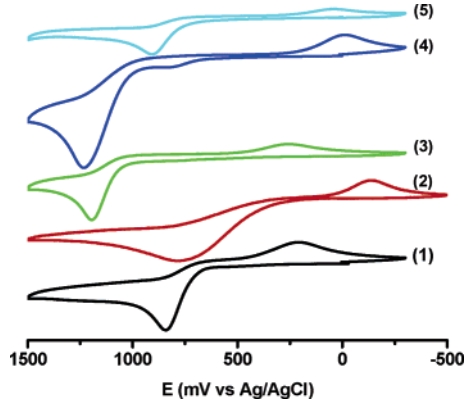

Figure 9. Cyclic voltammograms of **1**−**5** in acetonitrile ($C = 1 \times 10^{-3}$ mol·L^{-1}, at 22 ± 1 °C, 0.1 mol·L^{-1} $TBAClO_4$ as the supporting electrolyte, glassy carbon working electrode, platinum wire auxiliary electrode, and Ag/AgCl reference eletrode) at a scan rate of 100 mV·s^{-1}.

3.6. Cyclic Voltammetry. Cyclic voltammograms of complexes **1**−**5** were recorded in acetonitrile (0.1 mol·L^{-1} $TBAClO_4$) in the potential range +1800 to −1800 mV vs Ag/AgCl, and the data are presented in Table 3 and Figure 9. Cyclic voltammograms at different scan rates were recorded, and as all of the complexes present the same behavior, only the data for complex **1** are shown in Figure S4.

All of the complexes exhibit an irreversible cathodic process varying from +800 to +1300 mV vs normal hydrogen electrode (NHE). These peaks can be assigned to the oxidation of Co^{II} to Co^{III}, and the electrochemical irreversibility is attributed to an EC process (electrochemical

followed by a chemical process) related to the rearrangement of the geometry around the metal center probably changing from a trigonal bipyramidal to an octahedral structure when Co^{II} is oxidized to Co^{III}. Cyclic voltammograms were reversed immediately upon the oxidation process at different scan rates (Figure S5), and reversibility was not observed.

Complexes **1**−**5** present anodic waves that are tentatively attributed to the Co^{III} to Co^{II} reduction of the six-coordinate species generated in the EC process.

4. Discussion

4.1. Structural Remarks. As presented before, complexes **1** and **2** differ in the five- vs six-coordination of the Co^{II} center. This can be tentatively attributed to the difference in the ionic radius of chlorine (99 pm) and oxygen (74 pm). As chlorine has a bigger ionic radius than oxygen, when it coordinates to the metal center it promotes enough steric hindrance enforcing the five-coordination. On the other hand, when the acetate group is coordinated to the Co^{II}, the metal center is still accessible to a small molecule such as water and a six-coordinate complex can be obtained. According to these data, it can be concluded that the $^{i}Pr_2TCMA^-$ ligand is not bulky enough to enforce the five-coordination, except in the presence of large anions. On the other hand, at least when coordinated to Co^{II}, the $BPZG^-$ ligand seems to enforce this stereochemistry, providing to the Co^{II} center a coordination mode similar to that observed for Fe/Mn SODs. As a macrocyclic ligand, $^{i}Pr_2TCMA^-$ enforces more strain than the tetradentate $BPZG^-$ resulting in a more distorted geometry. From this point of view, complex **2** supports the suggestion that small molecules are able to access the active site of the enzyme during the catalytic disproportionation cycle[2] making it six-coordinate. Therefore, as complexes **1**−**5** present the same N_3O donor set atoms observed in all of the crystallographically characterized Fe/Mn SOD, those represent the first corroborative structural models for these enzymes. Furthermore, as the Co-substituted SODs have not been structurally characterized by single-crystal X-ray analysis, we propose that their active site should be analogous to those reported for the other Fe/Mn SODs, in which the Co^{II} center lies in a trigonal bipyramidal geometry. To reinforce this proposal, it is worth emphasizing that, as observed for the enzyme,[7] just Co^{II} species were isolated in this work suggesting a similar ligand field for these complexes and the enzyme. In addition, complex **5** should structurally model the azide-bound derivative of Co-containing SODs.

4.2. Magnetism and Spectroscopy. The dependency of μ_{eff} (or of $\chi_M T$) on temperature for complexes **1**−**5** is shown in Figure S1. As mentioned, the μ_{eff} values at 300 K for **1** and **3**−**5** are in the range of 3.66−4.50 μB and similar to the spin-only value for high-spin Co^{II} in a trigonal bipyramidal geometry (3.87 μB, $S = {}^3/_2$). The decrease of μ_{eff} values (or of $\chi_M T$) with decreasing the temperature can be interpreted for mononuclear Co^{II} as a contribution of the orbital angular momentum.[28] In fact, when the spin and the orbital angular momenta exist independently, the expected μ_{eff} value is 5.20 μB ($\mu_{LS} = [L(L+1) + 4S(S+1)]^{1/2}$, $L = 3$ and $S = {}^3/_2$). The contribution of orbital angular momentum for these complexes should be due to the distorted trigonal bipyramidal geometries.

Complex **2** is the only six-coordinate complex in this series and presents the highest μ_{eff} value (4.56), which is typical for Co^{II} octahedral complexes with d^7 high-spin state.[25]

As CH_2Cl_2 is an inert solvent, the electronic properties of all the complexes are expected to agree with the structural (trigonal bipyramidal) and the magnetic data (Co^{II} high spin) since changes in their coordination spheres are not expected. In fact, the UV−vis spectra observed for **1** and **3**−**5** are in good agreement with those observed for the high-spin trigonal bipyramidal Co^{II} complexes,[26] while complex **2** presents a typical six-coordinate high-spin Co^{II} spectra[26] with lower molar extinction coefficient values than the other complexes. The fact that the spectra recorded in CH_3CN show high similarities with those in CH_2Cl_2 also suggests no changes in this solvent.

The UV−vis spectra of all the complexes in $^{i}Pr_2OH/H_2O$ present significant changes compared to those discussed above. Complexes **1** and **2** show similar spectra, but the spectrum of **1** is higher in intensity than that for **2**, which demonstrates similarities in the environments around the Co^{II} ions, where complex **1** is in lower symmetry than complex **2**. The same behavior is observed for complexes **3** and **4**. Although conclusive evidence regarding the geometry adopted by these complexes in this medium is difficult, it is suggested that the presence of an equilibrium between five- and six-coordinate species exists.

Comparison of the UV−vis data for all of the complexes shows no trend regarding the electronic effects of $^{i}Pr_2TCMA^-$ and $BPZG^-$ ligands. In fact, steric and electronic effects should have important contributions in both ligands, since $^{i}Pr_2TCMA^-$ is a macrocyclic based and $BPZG^-$ is a tripodal ligand.

The geometry adopted by high-spin Co^{II} complexes can be inferred by EPR according to the literature[29−30] and the following classification: (i) distorted octahedral, A_1 (or $A_{||}$) = 0.02 and $g_1 \neq g_2 \neq g_3$ (or $g_{||} > g_\perp$); (ii) distorted tetrahedral, no resolved hyperfine structure and $g_1 \neq g_2 \neq g_3$; (iii) trigonal bipyramidal, no resolved hyperfine structure and $g_\perp > g_{||}$; (iv) complexes of low symmetry, $A_1 = 0.01-0.02$ and $g_1 \neq g_2 \neq g_3$.

EPR spectra of complexes **1**−**5** were recorded in CH_2Cl_2/toluene (1:1), and the spectra at 4.5 K are presented in Figure 8. The spectra of **1** and **3**−**5** are axial ($g_\perp > g_{||}$) with no well-resolved hyperfine structure, consistent with the retention of the crystallographically observed trigonal bipyramidal geometry in solution. Additionally, the g values observed for these complexes are in the range of those expected for

(28) Hossain, M. J.; Sakiyama H. *Inorg. Chim. Acta* **2002**, *338*, 255−259.

(29) McGarvey, B. R. In *Transition Metal Chemistry*; Carlin, R. L., Ed.; Marcel/Dekker, Inc.: New York, 1966; Vol. 3, pp 89−201.

(30) Kennedy, F. S.; Hill, H. A. O.; Kaden, T. A.; Vallee, B. L. *Biochem. Biophys. Res. Commun.* **1972**, *48*, 1533−1539.

both distorted four-coordinate and trigonal bipyramidal compounds with the $\pm^3/_2$ state as the lowest in energy (i.e., $-D$).[27]

In ^{i}Pr$_2$OH/H$_2$O (1:1), complexes **3**−**4** also show axial spectra ($g_\perp > g_\parallel$) and no resolved hyperfine structure, nevertheless, as the peaks are very broad it suggests the presence of more than one species in solution, which agree with the UV−vis data (Figure S3).

The EPR from complexes **1** and **2** are more informative, and it is possible to observe the hyperfine structure because of the ^{59}Co nuclear spin ($I = {}^7/_2$). The hyperfine lines are centered at $g_3 \sim 6.0$ and are overlapping the g_2 signal. As their intensities are uneven, it demonstrates the presence of an equilibrium of species in solution,[31] which agree with the UV−vis data observed for complexes **1** and **2**. Our data allow us to classify the geometry of complexes **1** and **2**, according to the criteria presented before,[28,29] as distorted octahedral or another lower symmetry.

For all of the complexes, it was also observed that the signal intensity decreases with increasing temperature. This effect has been reported as a typical behavior of high-spin Co^{II} with extensive spin−orbit coupling where the low-lying doublet is populated.[7]

Co^{II}-substituted SOD presents an EPR spectrum (10 K) characterized by a $g_\perp = 4.5$ and an eight line hyperfine resonance at $g_\parallel = 2.00$ with an anisotropic hyperfine coupling constant $A_\parallel = 10.6$ mT. In addition, the same temperature-dependent behavior[7] was observed.

The data observed for complexes **3** and **4** agree very well with those of the enzyme, which strongly support the proposition that the active site of the Co^{II}-substituted SOD structurally resembles these models.

4.3. Electrochemistry. The redox behavior of complexes **1**−**5** clearly demonstrates the stabilization of the Co^{II} state in the ligand field provided by the ^{i}Pr$_2$TCMA$^-$ and BPZG$^-$ ligands. As observed in Table 3, complexes **3**−**5** show the E_c process cathodically shifted compared to complexes **1** and **2**, indicating that more stabilization is provided by the BPZG$^-$ ligand and suggesting that it has a more electron-withdrawing character than the ^{i}Pr$_2$TCMA$^-$.

As mentioned before, the electrochemical irreversibility displayed by all of the complexes is probably related to an electron-transfer process followed by a rearrangement of the geometry around the metal center for complexes **1** and **3**−**5**, which probably changes from trigonal bipyramidal to octahedral as Co^{II} is oxidized to Co^{III}. This process is also expected to be accompanied by a spin-state conversion. As a Co^{II} center (high spin, d^7) in a trigonal bipyramidal geometry is oxidized, it is expected to form a Co^{III} (low spin, d^6) in an octahedral geometry. For complex **2**, it is expected that the electron transfer is coupled to the spin exchange since it is already in a distorted octahedral environment. This same behavior has been reported[32] for other Co^{II} complexes containing pyrazole-based ligands, in which it is also observed that the potential values are more positive for pyrazole-based than for TACN ligands. As mentioned before, the anodic wave in complexes **1**−**5** are assigned to the Co^{III} to Co^{II} reduction of the octahedral species generated in the EC process.

The potentials observed for the Co$^{II/III}$ oxidation process in complexes **1**−**5** (Table 3) are similar to that observed for the high-constrained trigonal bipyramidal complex [Co^{II}(L4)Cl]PF$_6$ ($E_{1/2} = +1151$ mV vs NHE).[33] Nevertheless, they are higher than those reported for other Co^{II} complexes[34] in a trigonal bipyramidal geometry: [Co^{II}(L^5)$_2$(H$_2$O)] ($E_{1/2} = +480$ mV vs SCE), [Co^{II}(L^1)]·H$_2$O ($E_{1/2} = +60$ mV vs SCE), and other Co^{II} and Co^{III} octahedral complexes [Co^{II}(L^1)Cl$_2$] ($E_{1/2} = +173$ mV vs NHE),[33] [Co^{II}(L2)Cl$_2$] ($E_{1/2} = -9$ mV vs NHE),[33] [Co^{II}(L3)Cl$_2$] ($E_{1/2} = -157$ V vs NHE),[33] [Co^{III}((*R*)-Metacn)(tacn)]$^{3+}$ ($E_{1/2} = -41$ mV vs NHE),[35] and [Co^{III}(tacn)$_2$]$^{3+}$ ($E_{1/2} = -41$ mV vs NHE).[36]

As mentioned, the complexes reported here are the first corroborative structural models of the Co^{II}-substituted SOD. Therefore, these are the first available redox potential data for examining the importance of potential on the inactivity of Co^{II}-substituted SODs. The results discussed above demonstrate the stabilization of the Co^{II} state by the N$_3$O-donor set of ligands used in this work. As the redox potentials to convert the Co^{II} to Co^{III} observed for complexes **1**−**5** are high, it can be inferred that the redox potential of the Co^{II}-substituted SOD may be outside the range required to convert the superoxide radical ($O_2^{\bullet-}$) to hydrogen peroxide. This observation provides a sufficient explanation for the inactivity of this Co^{II}-substituted enzyme.

5. Conclusion

In summary, we have synthesized and characterized two new N$_3$O-donor ligands which were used to obtain five new Co^{II} complexes (**1**−**5**). The complexes were characterized by several techniques. X-ray crystallographic analyses of all of the complexes revealed that we have synthesized the first corroborative structural models for the Co^{II}-substitued SOD. EPR results agree with those of the enzyme and also suggest that the active site of the enzyme resembles these models. Finally, we have demonstrated that the ligand field provides the stabilization of the Co^{II} state in a redox potential that is sufficient to explain the inactivity of the enzyme.

Acknowledgment. The authors are grateful for Grant GM39406 provided by the National Institutes of Health for support of this research.

Supporting Information Available: Crystallographic data in CIF format and additional table and figures. This material is available free of charge via Internet at http://pubs.acs.org.

IC050281H

(31) Tubbs, K. J.; Szajna, E.; Bennett, B.; Halfen, J. A.; Watkins, R. W.; Arif, A. M.; Berreau, L. M. *J. Chem. Soc., Dalton Trans.* **2004**, 2398−2399.
(32) Alwis, D. C. L. D.; Schultz, F. A. *Inorg. Chem.* **2003**, *42*, 3616−3622.
(33) Hubin, T. J.; Alcock, N. W.; Clase, H. J.; Seib, L. L.; Busch, D. H. *Inorg. Chim. Acta* **2002**, *337*, 91−102.
(34) Patra, A. K.; Ray, M.; Mukherjee, R. *J. Chem. Soc., Dalton Trans.* **1999**, 2461−2466.
(35) Küppers, H.-J.; Neves, A.; Pomp, C.; Ventur, D.; Wieghardt, K.; Nuber, B.; Weiss, J. *Inorg. Chem.* **1986**, *25*, 2400−2408.
(36) Wieghardt, K.; Schmidt, W.; Herrmann, W.; Küppers, H.-J. *Inorg. Chem.* **1983**, *22*, 2953−2956.